

Study of the Presence and Copper Content in the Properties of Cerium Oxide Destined for Photocatalysis

Maria Luiza Andrade da Silva¹, Marie Lídio dos Santos Galvão Ribeiro², Kimberly Paim Abeyta², Carlos Augusto de Moraes Pires³ and Sirlene Barbosa Lima³

¹ Chemistry Institute, Federal University of Bahia (UFBA), Brazil

² Salvador University (UNIFACS), Brazil

³ Polytechnic School, Federal University of Bahia (UFBA), Brazil

ABSTRACT

Due to the increasing discharge of organic pollutants into water resources, the treatment of pollutants has become a global priority. Photocatalysis has been used in the degradation of organic compounds because it uses a clean energy source and allows the degradation of pollutants in milder conditions. Cerium oxide has properties suitable for use as a photocatalyst and its performance can be improved with the addition of another metal oxide. In this context, the article aims to evaluate the influence of the presence and copper content on the properties of cerium oxide. The materials were characterized by FTIR, XRD, surface area measurement by BET method and spectroscopy in the UV-Vis region. It was verified that the presence of copper increased the crystallinity of the materials and conserved the cubic phase of cerium oxide, regardless of the content. On the other hand, it led to a decrease in the specific surface area of solids. In addition, the presence of copper favored radiation absorption and decreased the band gap energy of solids, and it can be concluded that the presence of copper improves the photocatalytic properties of catalysts based on cerium oxide.

Keywords – photocatalysis, cerium oxide, copper oxide, advanced oxidative processes

Date of Submission: 26-10-2020

Date of Acceptance: 05-11-2020

I. INTRODUCTION

Industrial development and the increase in the world's population stand out as the main responsible for environmental pollution caused by organic contaminants and various hazardous wastes. The continuous discharge of organic pollutants into water resources leads to water pollution and may affect human health and marine life [1,2]. The Lancet Commission on Pollution and Health estimates that about 1.8 million deaths worldwide are related to contaminated water [3]. Given this scenario, the treatment of pollutants has become a global priority [1,2].

Several methods have been developed for the removal or degradation of pollutants, such as adsorption, biodegradation, photocatalytic oxidation, among others [1,2,4]. Among them, advanced oxidative processes have stood out, as they promote the complete mineralization of pollutant molecules existing in industrial effluents from the formation of highly reactive oxidizing species for oxidation of pollutants [2,4-6]. Among the existing POAs, photocatalysis was promising due to its low cost, high efficiency and stability, in addition to its

mechanism enabling the use of sunlight as a source of clean energy, enabling the degradation of pollutants in milder conditions [1,2,7]. It is a technique that uses the concept of acceleration and increased yield of oxidation reactions through the combined use of catalysts, photosensitive conductors, and UV radiation. This radiation will cause the movement of the electron present in the valence band to the conduction band, inducing the creation of reducing and oxidizing sites, which promotes the degradation of polluting compounds. In addition, it allows the formation of free radicals, which will act in the degradation of pollutants [2, 8, 9].

Cerium oxide is a promising solid for use in photocatalysis due to its high ability to store oxygen in the network, resistance to photocorrosion and high photocatalytic activity. In addition, it presents high stability in the reaction and also electronic and optical properties, due to the presence of electrons 4f [2, 9, 10]. On the other hand, cerium oxide has a band gap in the range of 3.0-3.4 eV and, consequently, its application only using visible or solar light is restricted requiring activation by UV light. Thus, to increase its photocatalytic

performance, several approaches have been used, such as the association of cerium oxide with other oxides or metals [9, 11].

In this context, the present work aims to evaluate the influence of the presence and copper content on the properties of cerium oxide, aiming at application in photocatalysis.

II. MATERIAL AND METHODS

The support (cerium oxide) was prepared by the combustion method, in which the urea (50% excess in mass) was placed in a porcelain crucible under heating until its fusion. After a solution of the precursor salt ($\text{Ce}(\text{NO}_3)_3 \cdot 6\text{H}_2\text{O}$ 99% purity) was added to the crucible and the final solution was homogenized. The system was heated until there was the formation of a self-sustaining flame and a powder-shaped solid, which was macerated. Copper oxide was also synthesized for comparison by the same method. However, the precursor salt ($\text{Cu}(\text{NO}_3)_2 \cdot 3\text{H}_2\text{O}$ 99.5% purity) was placed to melt before the addition of the urea solution. The samples of cerium oxide and copper oxide were named as Ce and Cu samples, respectively.

The copper catalysts supported in cerium were prepared by varying the percentage of mass copper (3, 5 and 7%) and were named 3CuCe, 5CuCe and 7CuCe, respectively. Cerium oxide was impregnated with copper nitrate solutions, using an impregnating solution volume of $1.5 \text{ mL} \cdot \text{g}^{-1}$ of support. The system was kept under stirring and heating (80°C) until the solvent was completely evaporated. Then, the material was dried for 12 hours at 120°C and the solid was calcined under synthetic air flow from room temperature to 500°C , with heating rate of $10^\circ\text{C}/\text{min}$, for 2 hours.

The obtained solids were characterized by fourier transform infrared spectroscopy (FTIR), using a Shimadzu spectrometer and were obtained by dilution of a small part of the sample in potassium bromide (KBr); X-ray diffraction (XRD), by exposing the samples to a source of copper radiation, through a current of 30 mA, voltage of 40kV, scan interval of $20^\circ \leq 2\theta \leq 80^\circ$, and scanning speed of $2^\circ/\text{min}$; measurement of surface area by BET method with nitrogen adsorption and molecular absorption spectroscopy in the ultraviolet and visible region (UV/Vis). The band gap calculation of the samples was made using the Kubelka-Munk method based on Equation 1, in which R is the reflectance obtained through the molecular absorption spectrum. From the calculation of this function, an F(R) graph was plotted as a function of $h\nu$, in which $h\nu$ is the energy of the photon corresponding to each R observed, h is the Planck constant and ν is the frequency of the incident radiation in each R measured. From this graph, the band gap (E_g)

energy is used by the intersection of linear extrapolation of the spectrum with the abscissa [12].

$$F(R) = \frac{(1 - R)^2}{2R} \quad (1)$$

III. RESULTS AND DISCUSSION

The infrared spectra of the Ce and Cu samples and the calcined (5CuCe-C) and non-calcined (5CuCe-SC) samples presented similar profiles, as shown in Fig. 1. The bands located at 550 cm^{-1} in the spectra of all samples are associated with the stretching of the O-Ce-O bond, which confirms the nature of the material [13]. The bands in 1388 cm^{-1} present in the spectra of the Ce and 5CuCe-SC samples are related to the symmetrical stretching of the N-O bond, referring to the presence of nitrates [14]. In the spectrum of the 5CuCe-C sample, this band is inexpressive, which proves the efficiency of calcination in nitrate removal. The bands present in the range of 1621 cm^{-1} refer to physical adsorption of water molecules on the surface of solids [15]. The bands found in the range of 3436 cm^{-1} in the spectra of the Ce, Cu and 5CuCe-SC samples point to the stretch of the O-H bond referring to the presence of water in the sample [16]. On the other hand, in the spectrum of the 5CuCe-C sample, these bands were less expressive; evidencing that calcination was also effective in the removal of water from the surface of solids. The spectrum of the Cu sample presented a much higher number of bands than those seen in the other spectra (Fig. 1a).

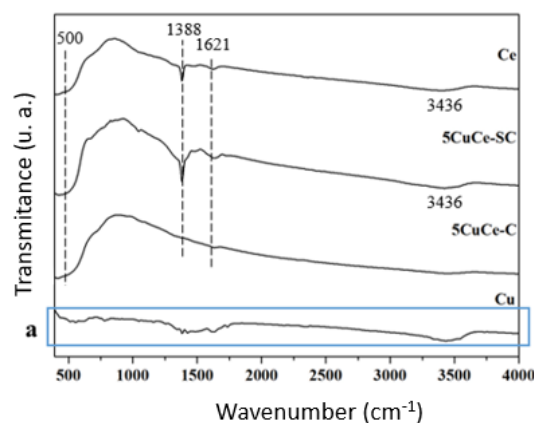


Figure 1. Spectra in the infrared region of the calcined Ce, Cu and 5CuCe samples (C) and 5CuCe uncalcined (SC).

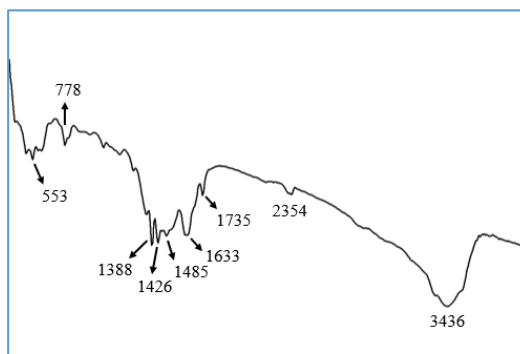


Figure 1a. Cutout of the spectrum in the infrared region of the Cu sample.

The band at 553 cm^{-1} indicates the vibration of the Cu-O bond, present in copper oxide II (CuO). On the other hand, the band present at 778 cm^{-1} is attributed to the vibration of the Cu-O bond found in copper oxide I (Cu_2O) [17, 18]. The band shown in 1378 cm^{-1} is related to the symmetrical stretch of the N-O bond, which indicates the presence of nitrates [14]. The bands present in 1426 and 1735 cm^{-1} correspond to the asymmetric stretch of the C-N bond [19] and the carboxylater group (C=O) [17], respectively, characteristic of urea. The band at 1485 cm^{-1} is related to the vibration of the asymmetric stretch of the O-NO₂ bond, which indicates the presence of copper hydroxide nitrate, also known as rouaite ($\text{Cu}_2(\text{NO}_3)(\text{OH})_3$) [20]. The band observed at 1633 cm^{-1} indicates the vibration of the O-H bond, related to the physical adsorption of water molecules on the surface of solids. The band present at 2354 cm^{-1} is related to the stretch of the C=O bond, which indicates the presence of CO₂ on the surface of the material, one of the combustion products. The band found at 3436 cm^{-1} is related to the stretch of the O-H bond due to the presence of water in the sample [15].

The X-ray diffractogram of the samples are shown in Fig. 2. The diffractogram of the Ce sample presented peaks (28° , 32° , 47° , 56° , 59° , 69° , 76° and 79°) corresponding to the cubic structure of cerium oxide IV (CeO_2), according to JCPDS 81-0792. These same peaks were evidenced in the diffratograms of samples 3CuCe, 5CuCe and 7CuCe, indicating that the presence of copper did not alter the cubic structure of cerium oxide IV. However, the presence of copper increased the crystallineness of solids, since the peaks found in the diffratograms of the impregnated samples were higher than those found in the Ce sample. In the diffratogram of the 7CuCe sample it is also possible to observe two peaks at 35° and 38° , related to the monoclinic structure of copper oxide II (CuO), in accordance with JCPDS 80-1917. It can be suggested that

copper oxide II (CuO) lies in a segregated phase in the cerium oxide network.

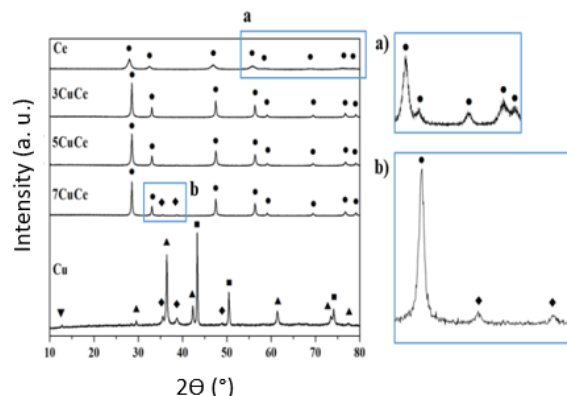


Figure 2. X-ray diffratograms of solids. (●) cubic phase of cerium oxide (CeO_2); (◆) cubic structure of copper oxide II (CuO); (▼) monoclinic structure of cerium hydroxide nitrate or rouaite ($\text{Cu}_2(\text{NO}_3)(\text{OH})_3$); (▲) cubic structure of copper oxide I (Cu_2O); (■) cubic phase of metallic copper (Cu).

The diffratogram of the Cu sample presented peaks referring to different copper materials, in addition to copper oxide II (CuO). The peaks at 43° , 50° and 74° correspond to the cubic structure of metallic copper (JCPDS 04-0836). On the other hand, the peaks present at 29° , 36° , 42° , 61° , 73° and 77° are associated with the cubic structure of copper oxide I (Cu_2O) (JCPDS 78-2076). The existing peaks at 35° , 38° and 48° , in turn, are linked to the monoclinic structure of copper oxide II (CuO) (JCPDS 80-1917). Finally, the peak presented at the 12° angle is related to the monoclinic structure of $\text{Cu}_2(\text{NO}_3)(\text{OH})_3$, a copper hydroxyl nitrate.

The values of the specific surface area of the synthesized samples are presented in Table 1. It can be observed that the presence and increase of the copper content caused a decrease in the specific surface area of solids. This may be associated with the calcination process done after the impregnation of copper, which may have led to the particles sintering, justifying the decrease in the area. On the other hand, the catalysts presented values of specific surface area higher than of pure copper oxide, used as a reference.

Table 1. Specific surface area values of synthesized samples.

Sample	Sg (m^2/g)
Ce	77
3CuCe	28
5CuCe	23
7CuCe	12

Cu	4
----	---

Fig. 3 shows the absorption spectra in the ultraviolet radiation region (200 to 400 nm) and in the visible range (400 nm to 700 nm) of solids. It is known that cerium oxide has a strong absorption in the ultraviolet region up to the wavelength of 400 nm and that the absorption bands are sensitive to the chemical environment and the presence of Ce^{3+} and Ce^{4+} ions. The UV spectrum of cerium oxide has three bands in the range of 200-350 nm, attributed to the transfer of charge between oxygen and cerium (Ce-O) and involving Ce^{4+} ions from the surface with different coordination numbers, which can vary between four and eight [14, 21]. The load transfer transition between Ce^{3+} and Ce^{4+} has been used to evaluate the oxygen storage capacity of cerium oxide. In the Ce sample spectrum, absorption bands were found at 225, 268 and 348 nm associated with the transition $O^{2-} \rightarrow Ce^{3+}$, $O^{2-} \rightarrow Ce^{4+}$ and transition between bands, respectively. The absorption referring to the transition $O^{2-} \rightarrow Ce^{4+}$ is slightly higher than that of the transition $O^{2-} \rightarrow Ce^{3+}$, which indicates the presence of the redox pair Ce^{3+}/Ce^{4+} with a slight inclination to the oxidation state +4 [14, 21, 22]. In the Cu sample spectrum, the absorbance profile is similar to that of the Ce sample, except in the visible region, in which the absorbance of the Cu sample is more expressive than that found in the Ce sample. Absorption bands were evidenced in 225, 268 and 514 nm. The first is related to the direct transition of electrons in CuO, the second refers to transitions between metal bands and the third is related to the d-d transition of Cu^{2+} ions in this region [23, 24]. The spectra of the samples impregnated with copper presented a profile similar to that found in the spectrum of the Ce sample, in the UV region. On the other hand, these samples showed greater absorbance in the visible range, which indicates that the presence of copper on the surface of the support favored the absorption of radiation. This is even more evident in the spectrum analysis of the 7CuCe sample, which presents the highest absorbance profile in the two radiation ranges, which indicates that the interaction between the cerium and copper is beneficial for the optical properties of the material.

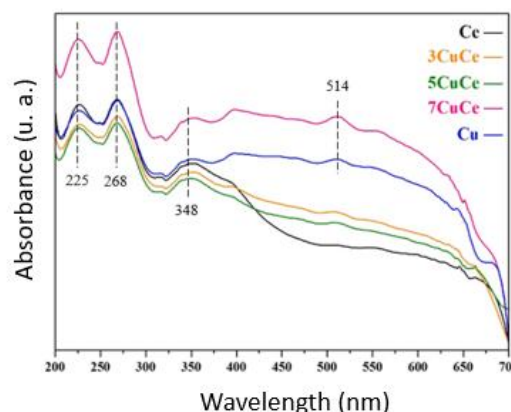


Figure 3. Spectra in the UV/Vis region of copper oxide and cerium samples (3CuCe, 5CuCe and 7CuCe), in addition to the samples of the pure oxides of each element (Cu and Ce, respectively).

The band gap energy values of solids are presented in Table 2. The presence of copper decreased the band gap energy of solids when compared to pure cerium oxide. The increase in copper content in the sample caused the greatest reduction of the material, so that the 7CuCe sample presented the lowest band-gap value among the others. This effect can be related to the synergy present in the cerium-copper interface, which makes radiation more easily absorbed, improving the properties of the photo catalyst [18].

Table 2. Band gap energy of synthesized samples, using the Kubelka-Munk method.

Sample	Eg (eV)
Ce	2,75
3CuCe	2,52
5CuCe	2,52
7CuCe	1,77
Cu	1,79

IV. CONCLUSION

Copper oxide catalysts supported on cerium oxide were synthesized to evaluate the influence of copper on the properties of cerium oxide. It was verified that the presence of copper increased the crystallineness of the materials and conserved the cubic phase of cerium oxide, regardless of the content. On the other hand, it led to a decrease in the specific surface area of solids. In addition, the presence of copper favored radiation absorption and decreased the band gap energy of solids, and it can be concluded that the presence of copper improves the photocatalytic properties of catalysts based on cerium oxide. Thus, copper and cerium oxide based catalysts can be expected to be promising for use in photocatalysis

ACKNOWLEDGEMENTS

The authors would like to thank FAPESB (Fundação de Amparo à Pesquisa do Estado da Bahia) and CNPq (Conselho Nacional de Desenvolvimento Científico e Tecnológico) for financial.

REFERENCES

- [1]. Z. Li, X. Meng, Z. Zhang, Recent development on MoS₂-based photocatalysis: A review, *Journal of Photochemistry and Photobiology C: Photochemistry Reviews* 35, 2018, 39–55
- [2]. R.S Pedanekar, S.K Shaikh, K.Y Rajpure, Thin film photocatalysis for environmental remediation: A status review, *Current Applied Physics*, vol 20, 2020, 931-952
- [3]. E. Boelee, G. Geerling, B. van der Zaan, A. Blauw, A. D. Vethaak, Water and health: From environmental pressures to integrated responses, *Acta Tropica* 193, 2019, 217-226.
- [4]. M. R .Al-Mamun, S. Kader, M. S. Islam, M. Z. H. Khan, Photocatalytic activity improvement and application of UV-TiO₂ photocatalysis in textile wastewater treatment: A review. *Journal of Environmental Chemical Engineering* 7, 2019, 103248.
- [5]. J. J. Rueda-Marquez, I. Levchuk, P. F. Ibañez, M. Sillanpää, A critical review on application of photocatalysis for toxicity reduction of real wastewaters, *Journal of Cleaner Production*, 258, 2020, 120694.
- [6]. P. Chowdhury, S. Nag, A. K. Ray, Phenolic Compounds-Natural Sources, Importance and Applications (IntechOpen, 2017).
- [7]. F.C.S.M. Lopes, d.G.C. da Rocha, P. Bargiela, H. Sousa Ferreira, A.d.M. Pires, Ag/TiO₂ photocatalyst immobilized onto modified natural fibers for photodegradation of anthracene, *Chemical Engineering Science*, 227 2020, 115939.
- [8]. LANGFORD, C. H. Photocatalysis — A Special Issue on a Unique Hybrid Area of Catalysis. *Catalysts*, Calgary, v.2, 2012, p. 327-329.
- [9]. M. Bellardita, R. Fiorenza, L. Palmisano, S. Scire, Photocatalytic and photothermocatalytic applications of cerium oxide-based materials, in Salvatore Scire and Leonardo Palmisano (Ed.), *Cerium Oxide (CeO₂): Synthesis, Properties and Applications* (2020) 109-167
- [10]. A. S. Thill, F. O. Lobato, M. O. Vaz, W. P. Fernandes, V. E. Carvalho, E. A. Soares, F. Polleto, S. R. Teixeira, F. Bernardi, Shifting the band gap from UV to visible region in cerium oxide Nanoparticles, *Applied Surface Science* 528, 2020, 146860.
- [11]. K. S. Ranjith, C. L. Dong, Y. Lum Y. Huang, C. Chen, P. Saravanan, K. Asokan, R. T. R. Kumar, Evolution of Visible Photocatalytic properties of Cu doped CeO₂ nanoparticles: Role of Cu²⁺ Mediated Oxygen Vacancies and the Mixed Valence States of Ce Ions, *ACS Sustainable Chem. Eng.*, 2018.
- [12]. R. López, R. Gómez, Band-gap energy estimation from diffuse reflectance measurements on sol-gel and commercial TiO₂: a comparative study, *Journal of sol-gel science and technology*, v. 61, n. 1, 2012, p. 1-7
- [13]. D. M. D. M. Prabaharan, K. Sadaiyandi, M. Mahendran, S. Sagadevan, Structural, optical, morphological and dielectric properties of cerium oxide nanoparticles, *Materials Research*, v. 19, n. 2, , 2016, 478-482.
- [14]. M; Chelliah, J. B. B. Rayappan, U. M. Krishnan, Synthesis and characterization of cerium oxide nanoparticles by hydroxide mediated approach., *Journal of Applied Sciences*, v. 12, n. 16, 2012, 1734-1737.
- [15]. K. K. Babitha, A. Sreedevi, K. P. Pryanka, B. Sabu, T. Varghese, Structural characterization and optical studies of CeO₂ nanoparticles synthesized by chemical precipitation, *Indian Journal of Pure & Applied Physics*, v. 53, n. 9, 2015, 596-603.
- [16]. Y. H. Liu, J. C. Zuo, X. F. Ren, L. Yong, Synthesis and character of cerium oxide (CeO₂) nanoparticles by the precipitation method, *Metalurgija*, v. 53, n. 4, 2014, 463-465.
- [17]. W. C. J. Ho, Q. Tay, H. Qi, Z. Huang, J. Li, Z. Chen, Photocatalytic and adsorption performances of faceted cuprous oxide (Cu₂O) particles for the removal of methyl orange (MO) from aqueous media, *Molecules*, v. 22 ,2017, 677.
- [18]. V. Prakash, R. K. Diwan, U. K. Niyogi, Characterization of synthesized copper oxide nanopowders and their use in nanofluids for enhancement of thermal conductivity, *Indian Journal of Pure & Applied Physics (IJPAP)*, v. 53, 2015, 753-758.
- [19]. V. Pop, A. Krizza, M. Ilis, Synthesis and stability studies in physiological-like conditions of two urea complexes of copper (II) and manganese (II). *An. Univ. Bucuresti. Chim.*, v. 2, 2002, 63-68.
- [20]. B. Liu, One-dimensional copper hydroxide nitrate nanorods and nanobelts for radiochemical applications. *Nanoscale*, v. 4, 2012, 7194-7198.

- [21]. G. R. Rao, H. R. Sahu, XRD and UV-Vis diffuse reflectance analysis of $\text{CeO}_2\text{-ZrO}_2$ solid solutions synthesized by combustion method, *Journal of Chemical Sciences*, v. 113, 2001, 651–658.
- [22]. M. Sakar, R. Rajkumar, S. Tripathy, S. Malakumar, Effect of Gd dopant concentration on the defect engineering in ceria nanostructures, *Materials Research Bulletin*, v. 47, 2012, 4340–4346.
- [23]. S. Hamad, G. K. Podagatlapalli, S. P. Tewari, S. V. Rao, Synthesis of Cu_2O , CuCl , and Cu_2OCl_2 nanoparticles by ultrafast laser ablation of copper in liquid media, *Pramana – J.Phys*, 2014, 1-7.
- [24]. N. R. Dhineshababu, V. Rajendran, N. Nithyavathy, R. Vetumperumal Study of structural and optical properties of cupric oxide Nanoparticles, *Applied Nanoscience*, Vol. 6, 2016, 933–939.

Maria Luiza Andrade da Silva, et. al. “Study of the Presence and Copper Content in the Properties of Cerium Oxide Destined for Photocatalysis.” *International Journal of Engineering Research and Applications (IJERA)*, vol.10 (10), 2020, pp 58-63.